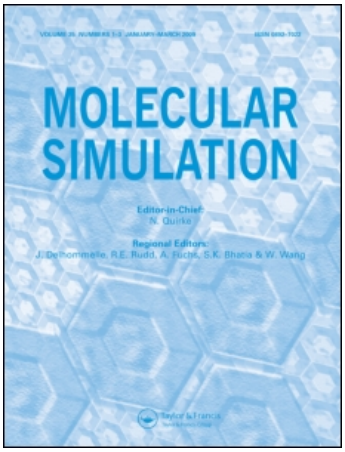

Molecular Simulation
Publication details, including instructions for authors and subscription information:
http://www.informaworld.com/smpp/title~content=t713644482

A computational analysis of pyrazole-based inhibitors binding to Hsp90 using molecular dynamics simulation and the MM-GBSA method

Chang-Hong Yi[ab]; Jian-Zhong Chen[a]; Shu-Hua Shi[a]; Guo-Dong Hu[a]; Qing-Gang Zhang[a]
[a] College of Physics and Electronics, Shandong Normal University, Jinan, China [b] Department of Mathematics and Physics, Shandong Jiaotong University, Jinan, China

Online publication date: 11 May 2010

To cite this Article Yi, Chang-Hong , Chen, Jian-Zhong , Shi, Shu-Hua , Hu, Guo-Dong and Zhang, Qing-Gang(2010) 'A computational analysis of pyrazole-based inhibitors binding to Hsp90 using molecular dynamics simulation and the MM-GBSA method', Molecular Simulation, 36: 6, 454 — 460
To link to this Article: DOI: 10.1080/08927021003628871
URL: http://dx.doi.org/10.1080/08927021003628871

Molecular Simulation
Vol. 36, No. 6, May 2010, 454–460

Taylor & Francis
Taylor & Francis Group

A computational analysis of pyrazole-based inhibitors binding to Hsp90 using molecular dynamics simulation and the MM-GBSA method

Chang-Hong Yi[ab], Jian-Zhong Chen[a], Shu-Hua Shi[a], Guo-Dong Hu[a] and Qing-Gang Zhang[a]*

[a]*College of Physics and Electronics, Shandong Normal University, Jinan 250014, China;* [b]*Department of Mathematics and Physics, Shandong Jiaotong University, Jinan 250023, China*

(*Received 13 May 2009; final version received 16 January 2010*)

Owing to the key role of heat-shock protein 90 (Hsp90) in the evolution, development and disease pathogenesis of cancer, it has been an important target for anti-cancer chemotherapy over the years. A five-nanosecond molecular dynamics simulation combined with the calculation of the binding free energy was carried out to investigate the binding mechanisms of three Hsp90 inhibitors 4BH, 2E1 and 2D9 to Hsp90. The binding free energy of each complex was computed using the molecular mechanics–generalised Born surface area method. Detailed binding free energies between each inhibitor and residues of Hsp90 were calculated using a per-residue basis decomposition method. The detailed inhibitor–residue interaction provides insights into binding mechanisms and in-depth understanding of the structure–affinity relationship. This study suggests that van der Waals energy is primarily responsible for driving the binding of the inhibitors to Hsp90, and the three inhibitors bind to Hsp90 in a similar binding mode. However, a substituent in 2D9 leads to higher binding free energy than the other two inhibitors. These data may assist in designing new potent drugs to combat cancer.

Keywords: absolute binding free energy; free energy decomposition; generalised Born model; MM-GBSA; Hsp90

1. Introduction

Heat-shock protein 90 (Hsp90) has emerged as a promising target for the treatment of cancer and other diseases. The function of Hsp90 is to chaperone the folding and then to maintain the stability of a number of 'client' proteins, including Her2, c-Kit, MET, Hif-1. As an ATP-dependent molecular chaperone, Hsp90 plays an important role in promoting cancer cell growth and/or survival [1–4]. Several small molecule inhibitors of Hsp90, such as the natural products geldanamycin and radicicol [4,5], have been discovered. A series of piperazinyl, morpholino and piperidyl of the pyrazole-based compounds [2,3,6,7] have been identified as novel Hsp90 inhibitors [8]. The most potent of the new compounds has a methylsulphonylbenzyl substituent that appends to the piperazine nitrogen.

The crystal structures of Hsp90 complexed with three inhibitors (4BH, 2E1 and 2D9) have been determined by X-ray crystallography. Figure 1 shows the structures of the three inhibitors. As can be seen in the figure, 2E1 is formed by appending an ethylamido group onto P1 in 4BH, while a methylsulphonylbenzyl substituent at position P2 turns 4BH into 2D9. Both substituents include hydrophobic groups, alkyl group or phenyl group, which may result in an increase in hydrophobic interactions. One purpose of this work is to assess the effects of these two substituents on binding free energy.

In this paper, we carried out nanosecond-level molecular dynamics (MD) simulation and free energy calculations to obtain information about the binding of 4BH, 2E1 and 2D9 to Hsp90. Calculation of the absolute binding energy was performed using the molecular mechanics–generalised Born surface area (MM-GBSA) [9,10] method to investigate the binding mode of the inhibitors and to explain their binding features. The energy decomposition method was also employed to study the interaction mechanisms between the inhibitors and Hsp90 at the atomic level, which helps to elucidate the structure–affinity relationship of the inhibitor–Hsp90 complexes. According to the analysis of the structural fluctuations, the calculations of the absolute binding free energy and the inhibitor–residue interaction spectra, we expected that the following two aims could be achieved: (1) to understand the mechanisms of the inhibitors binding to Hsp90 and (2) to study the effect of the structural differences between the three inhibitors on binding.

2. Theory and methods

2.1 MD simulation

Three PDB files were used as the initial structures of the inhibitor–Hsp90 complexes for the MD simulation: 2CCS.pdb for 4BH–Hsp90, 2CCT.pdb for 2E1–Hsp90 and 2CCU.pdb for 2D9–Hsp90. All the crystal water molecules in the PDB files were deleted. Hydrogen atoms

*Corresponding author. Email: zhangqg@sdnu.edu.cn

ISSN 0892-7022 print/ISSN 1029-0435 online

DOI: 10.1080/08927021003628871
http://www.informaworld.com

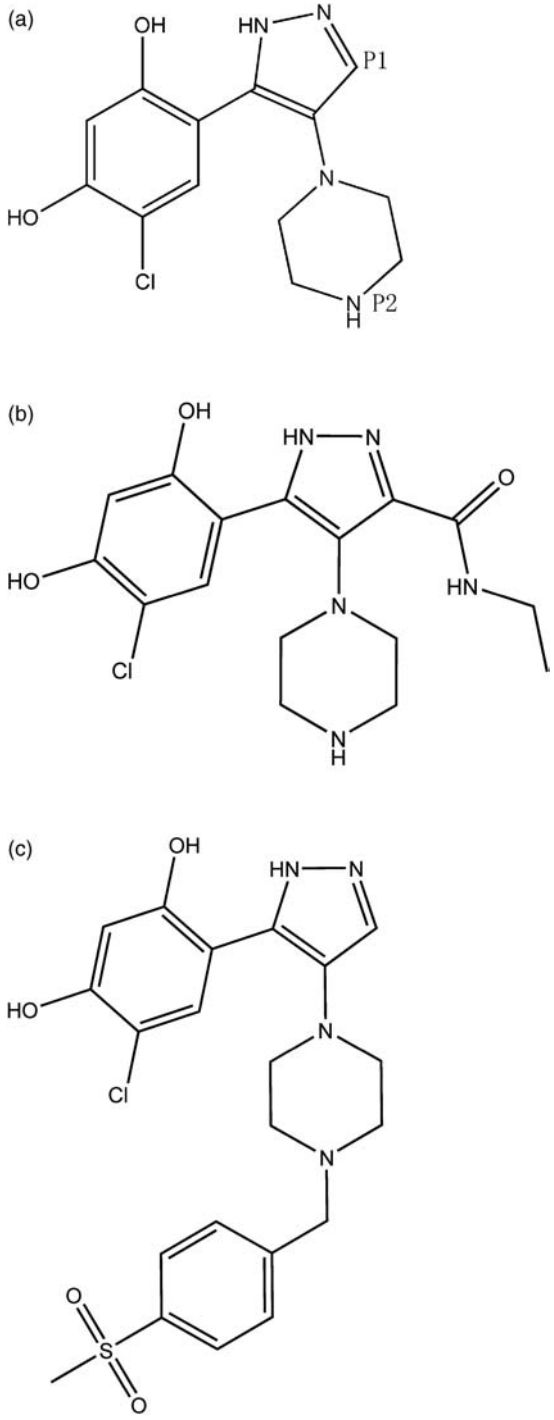

Figure 1. Molecular structures of the inhibitors: (a) 4BH, (b) 2D9 and (c) 2E1.

were added to the X-ray coordinates of the three inhibitors extracted from the inhibitor–Hsp90 crystal complex. The structural optimisations of the inhibitors at the Hartree–Fock/6-31G** level followed by a single-point calculation at the B3LYP/cc-PVTZ level were carried out using Gaussian03 to obtain the electrostatic potential. Partial charges and force field parameters for the inhibitors were generated automatically using the Antechamber program in AMBER 9.0 [11]. All MD simulations were accomplished using the AMBER 9.0 suite of programs with the ff03 force field [12]. Each complex was solvated in a periodic box filled by TIP3P water molecules. The closest distance from the surfaces of the water box to the solutes was set to be 10 Å. Eight Na^+ ions were placed around the inhibitor–Hsp90 complex to neutralise the charges of the system. The entire system was then minimised by three consecutive rounds, each round consisting of 500-step steepest descent and 1500-step conjugated gradient minimisation, in which harmonic constraints were applied to all non-hydrogen atoms of the complex with the strength of 100, 10 and 0 kcal/(mol $Å^2$), respectively. Such a stepwise procedure is aimed to resolve the close contacts between the complex and water molecules gradually.

After energy minimisation, the system was heated from 0 to 300 K in constant volume and equilibrated at 300 K for 100 ps. A five-nanosecond MD simulation was performed at a constant temperature of 300 K and a constant pressure of 1 atm without restriction on all the solute atoms. The particle-mesh Ewald method [13] was applied to calculate long-range electrostatic interactions in a periodic boundary condition. The Shake [14] method was used to constrain all of the covalent bonds involving hydrogen atoms. The time step for all MD simulations was set to 2 fs, with a non-bonded cut-off of 10 Å. Finally, conformations were collected every 10 ps for the last 1000 ps of the MD simulation, and the 100 snapshots collected were used for binding energy calculations.

2.2 The MM-GBSA calculation

The binding free energy can be used to scale the intensity of non-covalent interactions between two molecules. In this work, the binding free energies between the inhibitors and Hsp90 were calculated using MM-GBSA and normal mode analysis in AMBER 9.0. According to the thermodynamic cycle (Figure 2) [15], the absolute binding free energy in the solvent environment

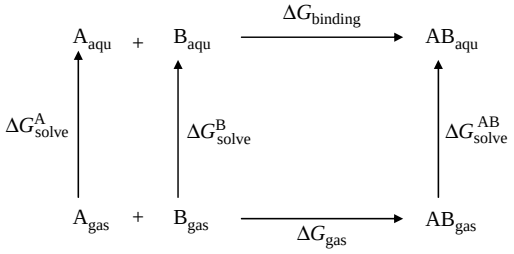

Figure 2. Thermodynamic cycle for absolute binding free energy calculation.

can be expressed as

$$\begin{aligned}\Delta G_{\text{binding}} &= \Delta G_{\text{gas}} - \Delta G^{\text{A}}_{\text{solve}} - \Delta G^{\text{B}}_{\text{solve}} + \Delta G^{\text{AB}}_{\text{solve}} \\ &\approx \Delta H_{\text{gas}} - T\Delta S + \Delta G^{\text{AB}}_{\text{solve}} - \Delta G^{\text{A}}_{\text{GBSA}} - \Delta G^{\text{B}}_{\text{GBSA}} \\ &\approx \Delta H_{\text{gas}} - T\Delta S + \Delta\Delta G_{\text{GB}} + \Delta\Delta G_{\text{SA}},\end{aligned} \tag{1}$$

where $\Delta G^{\text{A}}_{\text{solv}}$, $\Delta G^{\text{B}}_{\text{solv}}$ and $\Delta G^{\text{AB}}_{\text{solv}}$ are solvation free energies of A, B and AB, respectively, ΔG_{gas} and $\Delta G_{\text{binding}}$ are binding free energies in the gas phase and condensed phase, respectively. ΔH_{gas} is the total MM energy in the gas phase. The polar contribution to the free energy ($\Delta\Delta G_{\text{GB}}$) is calculated using the GB model of Tsui and Case [16] implemented in AMBER 9.0. The dielectric constant was set to be 1 inside the solute and 80 in the solvent in this work. The non-polar contribution to the solvation free energy ($\Delta\Delta G_{\text{SA}}$) is estimated by

$$\Delta\Delta G_{\text{SA}} = \gamma \times \text{SASA}, \tag{2}$$

where SASA is the solvent-accessible surface area (Å^2) that is calculated using the linear combination of pairwise overlaps [17] model. The value for the empirical constant γ, which represents surface tension, was set to 0.0072 kcal/(mol Å^2).

Finally, the entropy contribution to the free energy ($T\Delta S$) is determined from the equation

$$T\Delta S = T(\Delta S_{\text{trans}} + \Delta S_{\text{rot}} + \Delta S_{\text{vib}}), \tag{3}$$

where ΔS_{trans} and ΔS_{rot} are the entropy contributions from translational and rotational motion and were calculated using classic statistics mechanics [18]. The entropy contribution from vibrational motion (ΔS_{vib}) is obtained using normal mode analysis. Since the normal mode calculation of entropy for large systems is extremely time consuming, we applied only 25 snapshots taken from the last 1000 ps of MD simulations for each complex to estimate the entropy contribution. Each snapshot was minimised using the conjugated gradient method with a distance-dependent dielectric function $4R_{ij}$ (with R_{ij} being the distance between two atoms) until the root-mean-square of the energy gradient was lower than 10^{-4} kcal/(mol Å) [19].

3. Results and discussion

3.1 Equilibrium of the dynamics simulation

To assess the stability of three MD simulations, root-mean-square deviations (RMSDs) of the Hsp90 protein backbone atoms relative to the initial structures during the MD simulation were calculated (Figure 3). As shown in Figure 3, in the first 200 ps, the RMSD values increase quickly, which means that the structures of the three complexes dissolved in the solution relax, and repulsions are removed within the systems. One can see that the structure from the MD simulation is different from the initial structure. Figure 3 suggests that all three systems reach equilibrium after 500 ps of the MD simulation. The average RMSD values of 4BH–Hsp90, 2E1–Hsp90 and 2D9–Hsp90 complexes after the equilibrium are 1.126, 1.204 and 1.185 Å, respectively, and their deviations from the mean are lower than 0.59 Å, which shows that the dynamics stabilities of these systems are reliable.

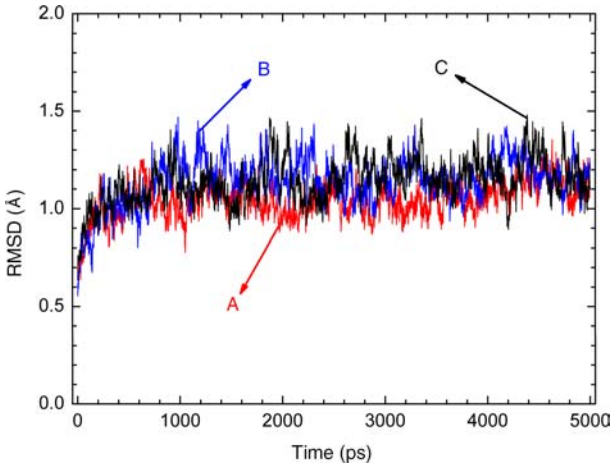

Figure 3. RMSD values of all C_α atoms on the backbone of the complexes during the MD simulation: (A) 4BH–Hsp90, (B) 2E1–Hsp90 and (C) 2D9–Hsp90.

3.2 Binding free energies calculated by MM-GBSA

The binding free energies were calculated by the MM-GBSA method using the single MD trajectory. The 100 snapshots were taken at intervals of 10 ps from the last 1000 ps of MD trajectories for the analysis of the binding free energy. Because the normal mode analysis was very time consuming, the normal mode analysis was carried out using 25 snapshots taken from the final 1000 ps of the MD trajectory. Table 1 summarises the components of MM and solvation energies computed by the MM-GBSA method. The binding free energies of 4BH, 2E1 and 2D9 to Hsp90 are −15.28, −19.77 and

Table 1. Binding free energies computed by the MM-GBSA method (kcal/mol).

Complex	ΔG_{ele}	ΔG_{vdw}	ΔG_{GB}	ΔG_{NP}	ΔG_{tot}	$-T\Delta S$	ΔG_{bind}	ΔG_{exp}[a]
4BH–Hsp90	−29.91	−36.61	37.69	−4.81	−33.64	18.36	−15.28	−6.96
2E1–Hsp90	−30.66	−44.93	42.60	−5.75	−38.73	18.96	−19.77	−7.11
2D9–Hsp90	−34.67	−57.63	50.05	−6.82	−49.07	23.03	−27.04	−8.05

Note: [a]The experimental binding free energies were calculated using IC_{50}, which were provided from Barril et al. [8].

−27.04 kcal/mol, respectively. It is so encouraging that the rank of the experimental affinities of the 4BH–Hsp90, 2E1–Hsp90 and 2D9–Hsp90 complexes is consistent with our predictions. We also noticed that the absolute values overestimate the binding affinities and the values of the calculated ΔG are about three times as much as the experimental data for the three inhibitors, which may be due to the use of the GB model. However, if the calculated binding affinities are scaled by a factor of about 3, the results will be in very good agreement with the experimental values. As can be seen from Table 1, van der Waals (ΔG_{vdw}) and electrostatic terms (ΔG_{ele}) in the gas phase are the main driving force of the inhibitor binding, whereas polar solvation energies (ΔG_{GB}) and entropy terms ($-T\Delta S$) oppose the binding. Non-polar solvation energies (ΔG_{NP}), which correspond to the burial of SASA upon binding, also drive the inhibitor binding slightly.

Table 2 reports the contributions of non-electrostatic and electrostatic interactions to the inhibitor–protein binding free energy. Despite the favourable electrostatic energies in the gas phase (Table 1), the contributions of polar solvation energies to binding are unfavourable for all three complexes, and the sum of ΔG_{ele} and ΔG_{GB} do not favour inhibitor binding to Hsp90 either. Table 2 also suggests that the net result of the non-electrostatic interaction, the sum of ΔG_{vdw} and ΔG_{NP}, is favourable for the binding of all three systems. It is noticeable that ΔG_{vdw} is almost 10 times stronger than ΔG_{NP}. Therefore, it is concluded that the binding free energies of this class of complexes are dominated by van der Waals energies rather than by electrostatic interactions.

As can be seen in Table 1, the inhibitor 4BH produces the weakest binding free energy (−15.28 kcal/mol) to Hsp90 among the three inhibitors. Compared with 4BH, the binding free energies of 2E1 and 2D9 to Hsp90 increase by 4.49 and 11.76 kcal/mol, respectively, which shows that the two substituents in positions P1 and P2 of 4BH intensify the binding of 2E1 and 2D9 to Hsp90. The methylsulphonylbenzyl substituent in position P2 of 4BH leads to a dramatic increase (−21.02 kcal/mol) in van der Waals energy of 2D9–Hsp90, while the *N*-ethyl amido substituent in position P1 of 4BH produces an increase in van der Waals energy of 2E1–Hsp90 by −8.32 kcal/mol. Although the favourable contribution of electrostatic energy also increases greatly in 2D9, this favourable effect is completely screened by the unfavourable solvation energy. As can be seen from the above analysis, two substituents in positions P1 and P2 of 4BH do intensify the binding of 2E1 and 2D9 to Hsp90.

Table 2. Contributions of non-electrostatic and electrostatic interactions to the inhibitor–protein binding free energies (kcal/mol).

Complex	4BH–Hsp90	2E1–Hsp90	2D9–Hsp90
Electrostatic ($\Delta G_{ele} + \Delta G_{GB}$)	7.78	11.94	15.38
Non-electrostatic ($\Delta G_{vdw} + \Delta G_{NP}$)	−41.42	−50.68	−64.45

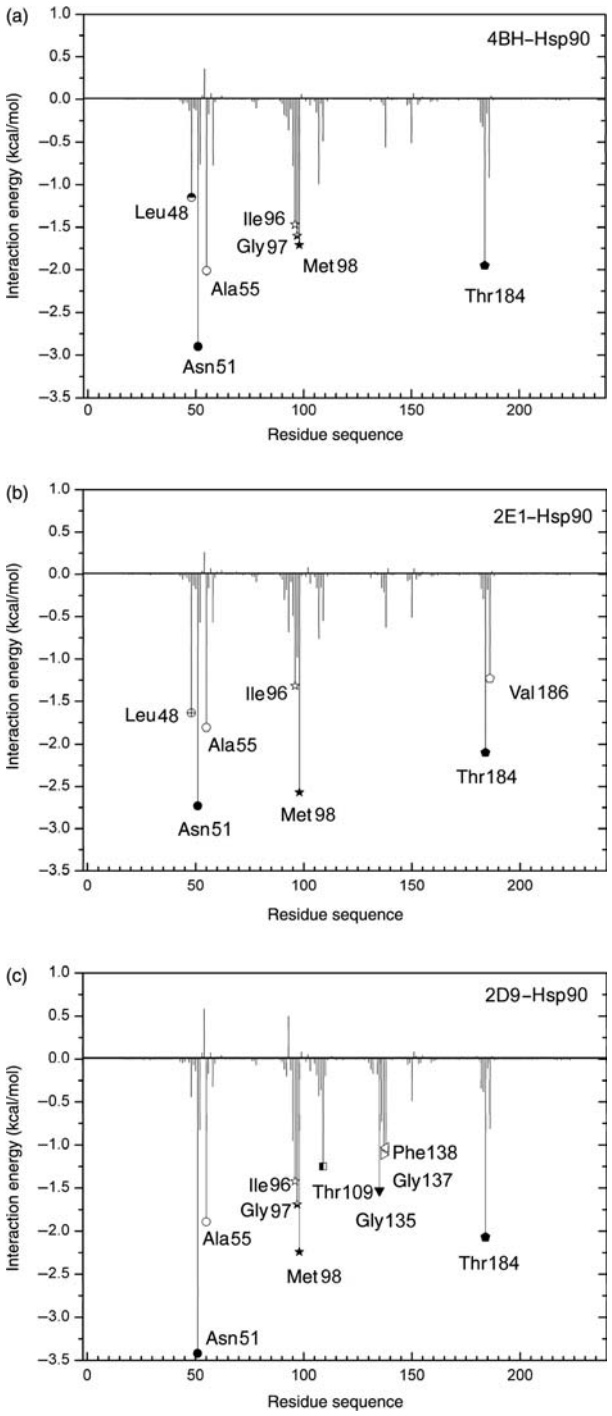

Figure 4. Inhibitor–residue interaction spectrum of (a) 4BH–Hsp90, (b) 2E1–Hsp90 and (c) 2D9–Hsp90 using the MM-GBSA method. The *x*-axis denotes the residue number of Hsp90 and the *y*-axis denotes the interaction energy between the inhibitor and specific residues.

Table 3. Contributions of the residues in an additional interaction region of 2D9–Hsp90 to the 2D9–Hsp90 binding free energies (kcal/mol).

Residues	ΔG_{ele}	ΔG_{vdw}	ΔG_{GB}	ΔG_{NP}	ΔG_{tot}
Gly135	−1.52	−1.07	1.20	−0.14	−1.53
Val136	−0.80	−0.67	0.74	−0.00	−0.73
Gly137	−1.43	−0.39	0.76	−0.05	−1.11
Phe138	0.29	−1.27	0.02	−0.07	−1.03
Sum	−3.46	−3.4	2.72	−0.26	−4.4

3.3 *Analyses of the structure–affinity relationship*

To obtain a more detailed insight into the mechanisms driving the binding of 4BH, 2E1 and 2D9 to Hsp90, an analysis of the structure–affinity relationship was carried out to complement the above energy analysis. The inhibitor–residue interaction spectra calculated by the MM-GBSA method are shown in Figure 4. The interaction spectra of the three inhibitors with Hsp90 are similar. The favourable residues can be divided into three groups around residues Asn51, Ile96 and Thr184. However, it is notable that the methylsulphonylbenzyl substituent at position P2 of 4BH generates an additional interaction region including the residues Gly135, Gly137 and Phe138 (Figure 4(c) and Table 3), which results in a total favourable contribution of −4.4 kcal/mol (Table 3), proving that the substituent plays an important role in the binding of 2D9 to Hsp90. Table 4 shows the decomposition of ΔG values on a per-residue basis into contributions from van der Waals energy, electrostatic interaction, polar solvation energy and non-polar solvation energy for residues with $|\Delta G| \geq 1.5$ kcal/mol for the three inhibitor–protein complexes. The contributions per residue were further subdivided into those from backbone atoms and those from side-chain atoms. Figure 5 displays the relative positions of the inhibitors in the lowest-energy structures of the binding complexes extracted from the MD simulation. Table 5 lists the information concerning hydrogen bonds formed between the three inhibitors and the residues of Hsp90.

For the 4BH–Hsp90 complex, the main favourable interactions come from five residues with $|\Delta G| \geq 1.5$ kcal/mol (Table 4 and Figure 4). As shown in Table 4, for all five residues, the van der Waals energy and non-polar solvation energy are favourable for binding. The main force driving the binding of 4BH to Asn51 is van der Waals energy (−2.83 kcal/mol). This result agrees well with the C—H···π interactions between the piperazine and benzodioxane of 4BH and the alkyl group in Asn51 (Figure 5(a)). The NH of pyrazole forms a hydrogen bond with the backbone carbonyl of Gly97, while the N2 atom forms a hydrogen bond with the hydrogen atom of the hydroxyl group of Thr184 (Table 5 and Figure 5(a)). These above hydrogen bonds were present in almost all of the published Hsp90 structures [20–24]. The distances between the corresponding donor and acceptor of the hydrogen bonds are 3.02 and 3.20 Å, respectively; thus, the main contribution of the electrostatic energy is an important driving force of 4BH binding to Gly97 and Thr84. In addition, the benzodioxane of 4BH contacts the alkyl group of Thr184 to form the C—H···π interactions (Figure 5(a)), thus the van der Waals energy also favours the binding of 4BH to Thr184 (Table 4). Similar to Asn51, the alkyl groups of Met98 and Ala55 also

Table 4. Decomposition of ΔG on a per-residue basis.

Residue	S_{vdw}	B_{vdw}	T_{vdw}	S_{ele}	B_{ele}	T_{ele}	S_{GB}	B_{GB}	T_{GB}	T_{SASA}	T_{GBTOT}
2CCS											
Asn51	−1.32	−1.5	−2.83	−0.43	0.47	0.04	0.77	−0.59	0.18	−0.29	−2.9
Ala55	−0.59	−0.77	−1.36	−0.08	0.12	0.04	0.06	−0.62	−0.56	−0.14	−2.01
Gly97	−0.06	−0.59	−0.65	−0.75	−0.36	−1.1	0.25	−0.08	0.17	−0.02	−1.6
Met98	−1.82	−0.25	−2.07	−0.47	0.36	−0.11	0.64	0.04	0.68	−0.2	−1.71
Thr184	−0.62	−0.24	−0.87	−0.37	−0.44	−0.82	−0.66	0.49	−0.17	−0.09	−1.95
2CCT											
Leu48	−0.62	−0.55	−1.17	0.01	−2.09	−2.09	−0.06	1.74	1.68	−0.05	−1.64
Asn51	−1.63	−1.52	−3.15	0.19	0.75	0.94	0.55	−0.75	−0.2	−0.33	−2.73
Ala55	−0.65	−0.6	−1.25	−0.03	0.04	0.01	0.02	−0.45	−0.43	−0.13	−1.81
Met98	−2.33	−0.45	−2.78	−0.08	−0.01	−0.08	0.3	0.23	0.53	−0.23	−2.57
Thr184	−1.1	−0.27	−1.37	0.03	−0.64	−0.61	−0.73	0.7	−0.03	−0.09	−2.1
2CCU											
Asn51	−2.72	−1.42	−4.14	−0.78	0.47	−0.31	1.97	−0.54	1.43	−0.41	−3.42
Ala55	−0.44	−0.89	−1.34	−0.13	0.07	−0.06	0.07	−0.43	−0.36	−0.13	−1.89
Gly97	−0.05	−0.43	−0.48	−0.79	−0.96	−1.75	0.21	0.35	0.56	−0.02	−1.69
Met98	−2.27	−0.39	−2.66	−0.37	0.4	0.03	0.67	−0.01	0.66	−0.27	−2.24
Gly135	0	−1.07	−1.07	−1.41	−0.11	−1.52	1.24	−0.04	1.2	−0.14	−1.53
Thr184	−0.55	−0.24	−0.8	−0.81	−0.34	−1.14	−0.43	0.39	−0.04	−0.09	−2.07

Notes: Energies are shown as contributions from the van der Waals energy (vdw), the electrostatic energy (ele), the polar solvation energy (GB), the non-polar solvation energy (SASA) of side-chain atoms (*S*), backbone atoms (*B*) and the sum of them (*T*) of the protein–inhibitor complex. Only the residues of $|\Delta G| \geq 1.5$ kcal/mol are listed. All values are given in kcal/mol.

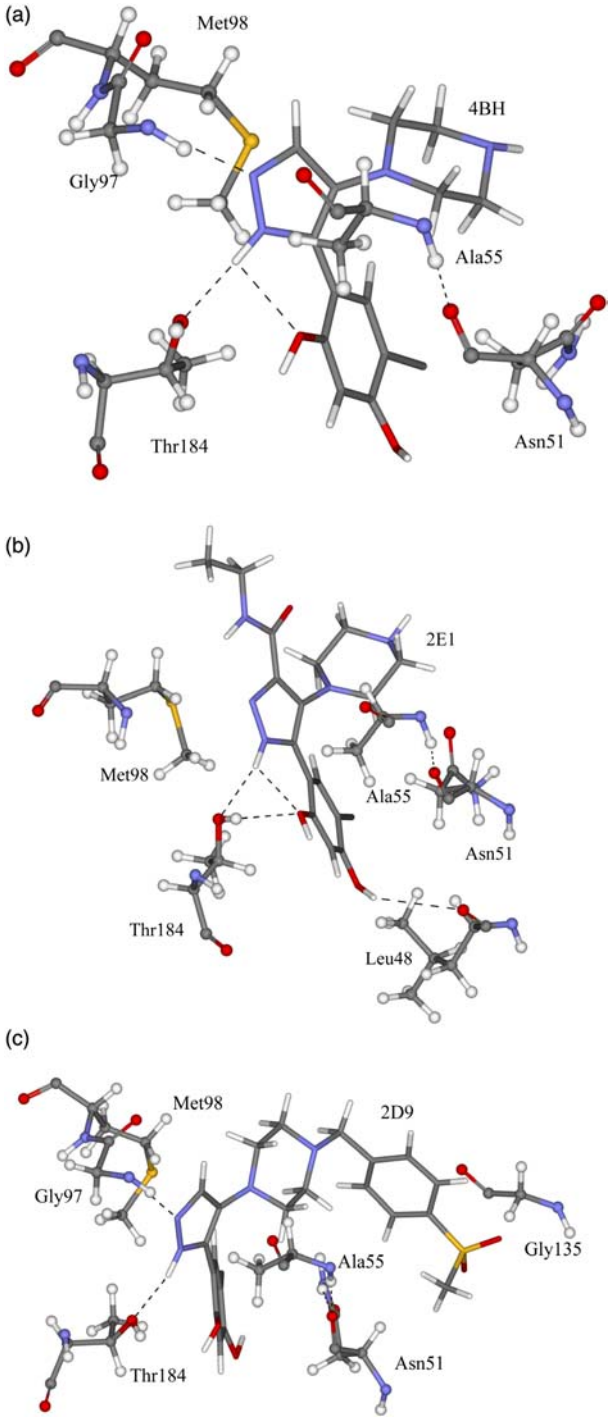

Figure 5. Geometries of eight residues, which produce some major interactions with (a) 4BH, (b) 2E1 and (c) 2D9, are plotted in the complex structures determined by the lowest-energy structures from the MD simulation. The hydrogen bonds are shown by the dashed line. The residues are indicated in a ball-and-stick representation. The three inhibitors are shown in a stick representation.

contact the pyrazole and benzodioxane of 4BH, respectively, to form the C—H···π interactions (Figure 5(a)), therefore it is mostly van der Waals energy that drives the binding of 4BH to Met98 and Thr184. It is concluded that the van der Waals energy and hydrogen bonds play a key role in the binding of 4BH to Hsp90.

As shown in Figure 4, the binding modes of 2E1 and 2D9 to Hsp90 are similar to that of 4BH. However, the substituents at positions P1 and P2 also produce some favourable differences compared to 4BH. In the 2E1–Hsp90 complex, the alkyl group of Met98 not only forms the C—H···π interaction with the benzodioxane ring as in 4BH, but also forms an additional C—H···H—C interaction with the alkyl group of the substituent (Figure 5(b)). This explains the increase in the van der Waals interaction between 2E1 and Met98 by 0.71 kcal/mol compared to that of 4BH (Table 4). The substitution in position P1 may produce a slight change in the orientation of 2E1 in the binding pocket, with two favourable outcomes: (1) 2E1 forms an additional hydrogen bond with Leu48; however, most of this favourable interaction is screened by the unfavourable polar solvation energy (Figure 5(b) and Table 5) and (2) the alkyl group of Leu48 produces a C—H···π interaction with the benzodioxane ring (Figure 5(b)), which is in agreement with the van der Waals energy of −1.17 kcal/mol in Table 4. In the 2D9–Hsp90 complex, the substitution in position P2 also brings two favourable changes: (1) compared to 4BH, the CH groups of Asn51 not only form the C—H···π interactions with the benzodioxane of 2D9, but also form additional C—H···H—C interactions and C—H···π interaction with the alkyl groups and phenyl groups of the substituent (Figure 5(c)), which agrees well with the increase of 1.31 kcal/mol in van der Waals interactions between 2D9 and Asn51 (Table 4); and (2) the substituent can interact with an additional residue Gly135 (Figure 5(c)), with a total contribution of 1.53 kcal/mol to binding free energy (Table 4). Based on the above analysis, it is concluded that the substituents at position P1 or P2 produce favourable contributions to the binding.

4. Conclusions

In this work, 5 ns MD simulations have been successfully carried out for 4BH–Hsp90, 2E1–Hsp90 and 2D9–Hsp90 complexes. The results suggest that the three complexes have similar RMSD fluctuations. The calculations of binding free energies for the three complexes using the MM-GBSA method show that van der Waals interactions drive the binding of all three inhibitors to Hsp90. The inhibitor–residue interaction spectrum from the energy decomposition shows that the methylsulphonyl-benzyl substituent in 2D9 results in an additional interaction region, which plays an important role in the binding of 2D9 to Hsp90. The analysis of the structure–affinity relationship proves that the substituents at position P1 or P2 can produce favourable contributions to the binding of 2E1 or 2D9 to Hsp90. These data may

Table 5. Hydrogen bonds formed by the three inhibitors with the residues of Hsp90.

Complex	Donor	Acceptor	D—A (Å)	D—H—A (°)	Frequency (%)
4BH–Hsp90	Thr184—OG1	4BH—N1—H5	3.02 ± 0.015	164.50 ± 8.64	100.0
	4BH—N2	Gly97—N—H	3.20 ± 0.015	134.27 ± 8.38	75.2
2E1–Hsp90	Thr184—OG1	2E1—N5—H16	3.15 ± 0.017	163.72 ± 9.47	93.2
	Leu48—O	2E1—O2—H18	3.06 ± 0.020	137.31 ± 11.99	58.4
2D9–Hsp90	Thr184—OG1	2D9—N4—H19	2.92 ± 0.011	163.96 ± 8.42	100.0
	2D9—N3	Gly97—N—H	3.05 ± 0.013	134.35 ± 8.35	87.2

be expected to assist in the development of potent inhibitors combating cancer.

Acknowledgements

This work was supported by the National Nature Science Foundation of China (No. 10874104) and the Key Project of Nature Science Foundation of Shandong Province (Z2007A05).

References

[1] L. Neckers and S.P. Ivy, *Heat shock protein 90*, Curr. Opin. Oncol. 15 (2003), pp. 419–424.
[2] P. Workman, *Overview: Translating Hsp90 biology into Hsp90 drugs*, Curr. Cancer Drug Targets 3 (2003), pp. 297–300.
[3] D.B. Solit, H.I. Scher, and N. Rosen, *Hsp90 as a therapeutic target in prostate cancer*, Semin. Oncol. 30 (2003), pp. 709–716.
[4] L. Whitesell, R. Bagatell, and R. Falsey, *The stress response: Implications for the clinical development of Hsp90 inhibitors*, Curr. Cancer Drug Targets 3 (2003), pp. 349–358.
[5] S.M. Roe, C. Prodromou, R. O'Brien, J.E. Ladbury, P.W. Piper, and L.H. Pearl, *Structural basis for inhibition of the Hsp90 molecular chaperone by the antitumor antibiotics radicicol and geldanamycin*, J. Med. Chem. 42 (1999), pp. 260–266.
[6] B.W. Dymock, X. Barril, P.A. Brough, J.E. Cansfield, A. Massey, E. McDonald, R.E. Hubbard, A. Surgenor, S.D. Roughley, P. Webb, P. Workman, L. Wright, and M.J. Drysdale, *Structure-based discovery of a new class of Hsp90 inhibitors*, J. Med. Chem. 48 (2005), pp. 4212–4215.
[7] I. Hostein, D. Robertson, F. DiStefano, P. Workman, and P.A. Clarke, *Inhibition of signal transduction by the Hsp90 inhibitor 17-allylamino-17-demethoxygeldanamycin results in cytostasis and apoptosis*, Cancer Res. 61 (2001), pp. 4003–4009.
[8] X. Barril, M.C. Beswick, A. Collier, M.J. Drysdale, B.W. Dymock, A. Fink, K. Grant, R. Howes, A.M. Jordan, A. Massey, A. Surgenor, J. Wayne, P. Workman, and L. Wright, *4-Amino derivatives of the Hsp90 inhibitor CCT018159*, Bioorg. Med. Chem. Lett. 16 (2006), pp. 2543–2548.
[9] G. Holger, K. Christina, and A.C. David, *Insights into protein–protein binding by binding free energy calculation and free energy decomposition for the Ras–Raf and Ras–RalGDS complexes*, J. Mol. Biol. 330 (2003), pp. 891–913.
[10] Y. Xu and R.X. Wang, *A computational analysis of the binding affinities of FKBP12 inhibitors using the MM-PB/SA method*, Proteins: Struct., Funct., Bioinform. 64 (2006), pp. 1058–1068.
[11] D.A. Case, T.A. Darden, T.E. Cheatham, III, C.L. Simmerling, J. Wang, R.E. Duke, R. Luo, K.M. Merz, D.A. Pearlman, M. Crowley, R.C. Walker, W. Zhang, B. Wang, S. Hayik, A. Roitberg, G. Seabra, K.F. Wong, F. Paesani, X. Wu, S. Brozell, V. Tsui, H. Gohlke, L. Yang, C. Tan, J. Mongan, V. Hornak, G. Cui, P. Beroza, D.H. Mathews, C. Schafmeister, W.S. Ross, and P.A. Kollman, *AMBER 9*, University of California, San Francisco, CA, 2006.
[12] Y. Duan, C. Wu, S. Chowdhury, M.C. Lee, G. Xiong, W. Zhang, R. Yang, P. Cieplak, R. Luo, T. Lee, J. Caldwell, J. Wang, and P. Kollman, *A point-charge force field for molecular mechanics simulations of proteins based on condensed-phase quantum mechanical calculations*, J. Comput. Chem. 24 (2003), pp. 1999–2012.
[13] T. Darden, D. York, and L. Pedersen, *Particle mesh Ewald: An N log(N) method for Ewald sums in large systems*, J. Chem. Phys. 98 (1993), pp. 10089–10092.
[14] H.P. Ryckaert, G. Ciccotti, and H.J.C. Berendsen, *Numerical integration of the Cartesian equations of motion of a system with constraints: Molecular dynamics of n-alkanes*, J. Comput. Phys. 23 (1977), pp. 327–341.
[15] J.M. Wang, P. Morin, W. Wang, and P.A. Kollman, *Use of MM-PBSA in reproducing the binding free energies to HIV-1 RT of TIBO derivatives and predicting the binding mode to HIV-1 RT of efavirenz by docking and MM-PBSA*, J. Am. Chem. Soc. 123 (2001), pp. 5221–5230.
[16] V. Tsui and D.A. Case, *Theory and applications of the generalized Born solvation model in macromolecular simulations*, Biopolymers 56 (2001), pp. 275–291.
[17] J. Weiser, P.S. Shenkin, and W.C. Still, *Approximate atomic surfaces from linear combinations of pairwise overlaps (LCPO)*, J. Comput. Chem. 20 (1999), pp. 217–230.
[18] H. Gohlke and D.A. Case, *Converging free energy estimates: MM-PB (GB) SA studies on the protein–protein complex Ras–Raf*, J. Comput. Chem. 25 (2003), pp. 238–250.
[19] D.A. Pearlman, *Evaluating the molecular mechanics Poisson–Boltzmann surface area free energy method using a congeneric series of ligands to p38 MAP kinase*, J. Med. Chem. 48 (2005), pp. 7796–7807.
[20] T.E. Barta, J.M. Veal, J.W. Rice, J.M. Partridge, R.P. Fadden, W. Ma, M. Jenks, L. Geng, G.J. Hanson, K.H. Huang, A.F. Barabasz, B.E. Foley, J. Otto, and S.E. Hall, *Discovery of benzamide tetrahydro-4H-carbazol-4-ones as novel small molecule inhibitors of Hsp90*, Bioorg. Med. Chem. Lett. 18 (2008), pp. 3517–3521.
[21] C.E. Stebbins, A.A. Russo, C. Schneider, N. Rosen, F.U. Hartl, and N.P. Pavletich, *Crystal structure of an Hsp90-geldanamycin complex: Targeting of a protein chaperone by an antitumor agent*, Cell 89 (1997), pp. 239–250.
[22] J.M. Jez, J.C. Chen, G. Rastelli, R.M. Stroud, and D.V. Santi, *Crystal structure and molecular modeling of 17-DMAG in complex with human Hsp90*, Chem. Biol. 10 (2003), pp. 361–368.
[23] C. Prodromou, S.M. Roe, R. O'Brien, J.E. Ladbury, P.W. Piper, and L.H. Pearl, *Identification and structural characterization of the ATP/ADP-binding site in the Hsp90 molecular chaperone*, Cell 90 (1997), pp. 65–67.
[24] B. Dymock, X. Barril, M. Beswick, A. Collier, A. Massey, N. Davies, M. Drysdale, A. Fink, C. Fromont, R.E. Hubbard, A. Massey, A. Surgenor, and L. Wright, *Adenine derived inhibitors of the molecular chaperone HSP90 – SAR explained through multiple crystal structures*, Bioorg. Med. Chem. Lett. 14 (2004), pp. 325–328.